$$F_2 = \tanh\left(\left(\max\left(2\frac{k^{1/2}}{\beta^* \omega y}, \frac{500\nu}{y^2\omega}\right)\right)^2\right) \tag{26}$$

$$S = \left(S_{ij}S_{ij}\right)^{1/2} \tag{27}$$

where F_1 and F_2 are the mixed functions used to determine which of the k-ω model and the k-ε model should be used for the calculation area.

3.2 Model coefficient adjustment

According to the rotation correction function proposed by Spalart, the turbulence energy generation term P_K of the turbulence model is corrected [12-13].

$$P_K \rightarrow P_K f \tag{28}$$

The dissipation term is corrected by the Hellsten's Richardson number correction model [14-15], and the correction coefficients for rotation and curvature are defined as follows:

$$F = \frac{1}{1 + C_{\mathrm{rc}} Ri} \tag{29}$$

$$Ri = \frac{|\omega_{ij}|}{|S_{ij}|}\left(\frac{|\omega_{ij}|}{|S_{ij}|} - 1\right) \tag{30}$$

where C_{rc}= 3.6, and ω_{ij} and S_{ij} are respectively the average rotational tensor and stress rate tensor of the motion, which are calculated by Formulas (6) and (7).

In light of Formulas (28) & (29), the corrected model is expressed as follows:

$$\frac{\partial K}{\partial t} + u_j \frac{\partial K}{\partial x_j} = P_K f_{\mathrm{r}} - \beta^* \omega K + \frac{\partial}{\partial x_i}\left[\left(\upsilon + \sigma_k \upsilon_{\mathrm{t}}\right)\frac{\partial K}{\partial x_i}\right] \tag{31}$$

$$\frac{\partial \omega}{\partial t} + u_j \frac{\partial \omega}{\partial x_j} = \gamma \frac{\omega}{K} P_K f_{\mathrm{r}} - F\beta\omega^2 + \frac{\partial}{\partial x_j}\left[\left(\upsilon + \sigma_\omega \upsilon_{\mathrm{t}}\right)\frac{\partial \omega}{\partial x_j}\right] - 2\left(F_1 - 1\right)\sigma_{\omega 2}\frac{1}{\omega}\frac{\partial K}{\partial x_j}\frac{\partial \omega}{\partial x_j} \tag{32}$$

where β^*=0.09, σ_k=2, γ=5/9, β=0.075, σ_ω=2, and $\sigma_{\omega 2}$=0.44. The ω of the boundary layer is calculated in combination with Formulas (18), (19) & (20),.

4. CALCULATION AND ANALYSIS

4.1 Data of case study

This paper applies the coefficient-corrected k-ω SST turbulence model to the flow field calculation of the centrifugal pump of automobile motor. The structural parameters are as follows: the blade z=7, the impeller diameter is18mm, the volute is involute, the minimum gap between the shell of volute tongue and the impeller is 0.5mm, and the minimum distance between the bearing surface and the impeller is 1mm. For better solution convergence, a triangular prism mesh network is pulled out from the outlet of water pump with long cooling circulation. The mesh is shown in Figure 1.

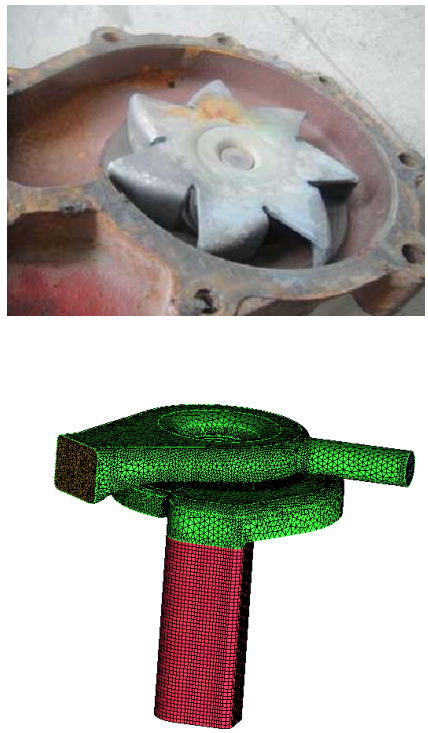

Figure 1. The mesh chart of the centrifugal pump

4.2 Calculation implementation and boundary conditions

The coefficients of the model's computational items are adjusted through dynamic loading of the solver by the UDF (User Defined Function) in the fluent software. The adjusted model is defined as k-ω SST—RCE.

The boundary conditions are set as follows:

The flow of coolant in the pump is regarded as a steady-state, adiabatic, incompressible turbulence; the inner wall of the pump is considered to be hydraulically smooth; the uncoupled implicit algorithm is adopted, with the second order of accuracy; the coolant's physical parameters are selected according to the test; the mass flow inlet and outflow outlet are chosen; the information transfer between the dynamic and static parts are treated by the GGI.

4.3 Calculation results and analysis

This paper applies the k-ω SST model (model 1) and k-ω SST—RCE model (model 2) to the steady-state turbulence computation of the centrifugal pump of the automobile motor under different working conditions. To avoid the interference from the mesh, the author designs 5 mesh division plans (Table 1). As shown in the table, the pump lift results of the two model only have slight changes when the mesh number is greater than 1.77 million. Thus, Plan 3 is adopted by this paper for follow-up study.

4.3.1 Characteristic data analysis

Table 2 displays the calculated results of characteristic data of the centrifugal pump at different rotating speeds and at different flows with a fixed speed, and lists the data of the centrifugal pump obtained in the test by the manufacturer.

Figure 2 to Figure 7 display the curves of the pump lift and efficiency calculated by the k-ω SST model and the k-ω SST—RCE model at different rotating speeds and at the design flow of Q, 0.8Q and 0.6Q, as well as the curves of the pump lift and efficiency measured in the test by the manufacturer.

It can be seen from the curves in Figures 2 to 5 that the results of both models stay close to the test curves, and the accuracy errors are within 5%. Comparatively speaking, the results of the *k-ω* SST—RCE model are closer to the test values. In the working condition of a rotating speed of 3,370n/min and a flow of 0.6Q, the results of the *k-ω* SST—RCE model are very similar to the test results. The calculated pump lift is 0.3% more accurate than that of the *k-ω* SST model, the calculated efficiency is about 0.7% more accurate than that of the latter.

Table 1. The mesh division plan and the calculation results

Plan	Mesh number (10^4)	The pump lift calculated by model 1 H/m	The pump lift calculated by model 2 H/m
1	136	16.11	16.65
2	154	18.09	17.20
3	177	18.12	18.03
4	199	18.18	18.06
5	221	18.17	18.05

Table 2. The experimental data and model calculation results

Group	N (n/min)	Q (L/min)	Measured pump lift (H/m)	H_1	H_2	ΔH_1 (H_1-H)	ΔH_2 (H_2-H)	ΔH_1/H(%)	ΔH_2/H(%)
1	3370	300	17.875	18.12	18.03	0.245	0.155	1.35	0.86
2	3370	240	19.81	20.13	20.05	0.32	0.24	1.59	1.20
3	3370	180	20.9	21.09	21.04	0.19	0.14	0.90	0.67
4	2500	240	10.56	11.08	11.02	0.52	0.46	4.69	4.17
5	2500	192	11.01	11.51	11.45	0.5	0.44	4.34	3.84
6	2500	144	12.19	12.6	12.47	0.41	0.28	3.25	2.25
7	2000	150	7.75	6.32	6.43	-1.43	-1.32	-22.63	-20.53
8	2000	120	8.03	6.96	6.87	-1.07	-1.16	-15.37	-16.89
9	2000	90	8.18	7.31	7.14	-0.87	-1.04	-11.90	-14.57
Group	N (n/min)	Q (L/min)	Measured efficiency (η/%)	η_1	η_2	$\Delta\eta_1$ (η_1-η)	$\Delta\eta_2$ (η_1-η)	$\Delta\eta_1$/η(%)	$\Delta\eta_2$/η(%)
1	3370	300	31	32.3	31.8	1.3	0.8	4.02	2.52
2	3370	240	28.4	29.3	28.9	0.9	0.5	3.07	1.73
3	3370	180	26	26.4	26.2	0.4	0.2	1.52	0.76
4	2500	240	35.3	36.7	36.2	1.4	0.9	3.81	2.49
5	2500	192	32.1	33.2	32.8	1.1	0.7	3.31	2.13
6	2500	144	26.8	27.7	27.5	0.9	0.7	3.25	2.55
7	2000	150	35.5	31.9	33.8	-3.6	-1.7	-11.29	-5.03
8	2000	120	31.1	29.8	28.6	-1.3	-2.5	-4.36	-8.74
9	2000	90	25.6	24.7	23.9	-0.9	-1.7	-3.64	-7.11

In Figures 6 and 7, the curves of the numerical results of the two models intersect each other. If the rotating speed remains at a low level, the numerical results of the k-ω SST—RCE are higher with a big flow, and lower with a small flow. Through comparison with the measured data, it is found that the calculated results of pump lift under different flow conditions all have errors of more than 10%, the biggest of which is up to 22.63%. The calculated results of efficiency under different flow conditions all have errors of more than 3%, the biggest of which is up to 11.29%. The errors are too large, and thus it is deemed that the results are not correct. In the causal analysis, in order to compare the calculation accuracy of different models, the same condition is set up for all working conditions – the flow field is steady on the interface between the rotating and stationary areas. However, when the pump rotates at a low speed, the rotating speed of the flow field in the pump decreases. The flow in the flow field is transient and pulsatile, and the flow on the interface between the rotating and stationary areas can no longer be regarded as steady and inhomogeneous, that is, it no longer satisfies the prerequisite for simulation with the MRF (Multiple reference frame) model, leading to large errors in the calculated results.

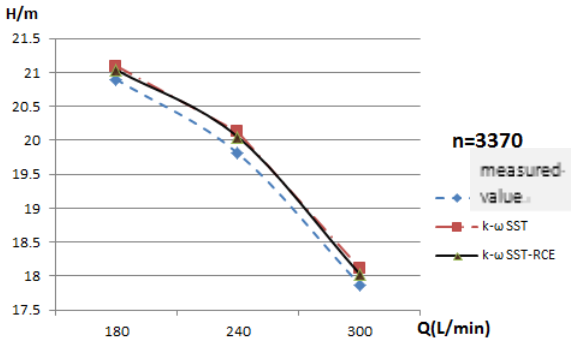

Figure 2. The pump lift curves at n=3,370/Q=300

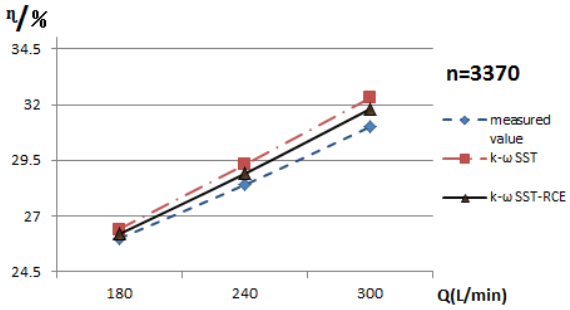

Figure 3. The efficiency curves at n=3,370/Q=300

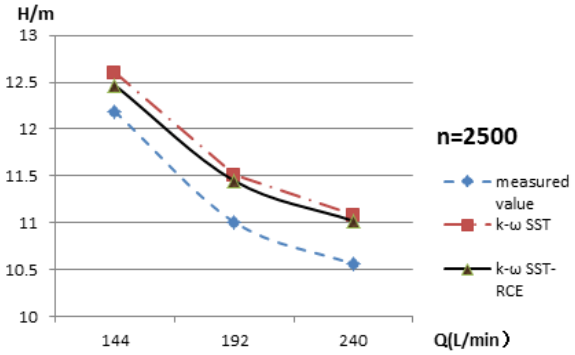

Figure 4. The pump lift curves at n=2,500/Q=240

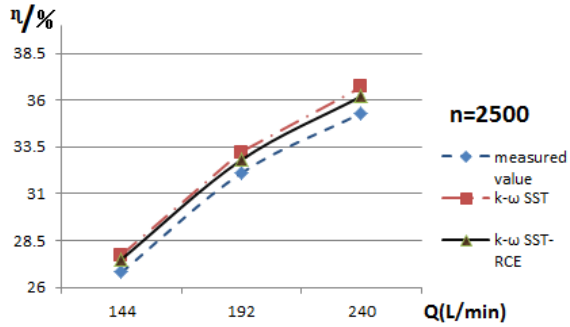

Figure 5. The efficiency curves at n=2,500/Q=240

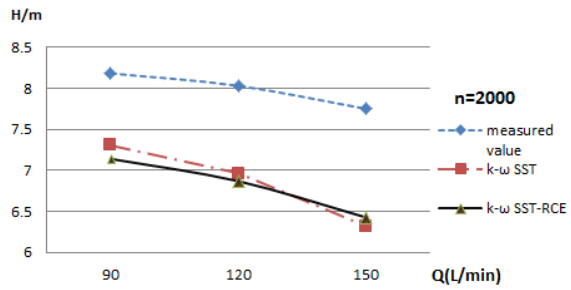

Figure 6. The pump lift curves at n=200/Q=150

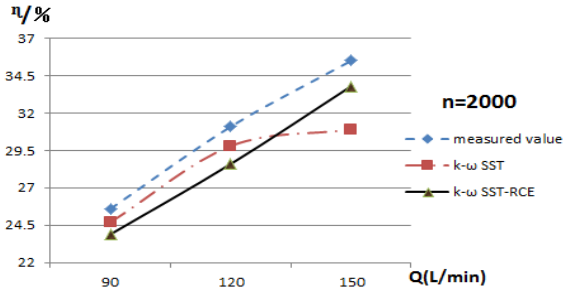

Figure 7. The efficiency curves at n=200/Q=150

4.3.2 Analysis of flow field results

The characteristic data analysis points out that, at a high rotating speed, the *k-ω* SST—RCE model (model 2) offers a better illustration of the motion of a fast rotating and highly curved flow field than the *k-ω* SST model (model 1). To make a comprehensive comparison between the characteristics and differences of the two models, the author chose to analyze the following three aspects of the flow field calculation at a rotating speed of 3,370n/min and a flow of 180L/min.

Turbulence intensity and viscosity analysis. Figures 8-11 shows the turbulence intensity and viscosity nephograms of the flow field. The trends of the two parameters are largely the same.

When it comes to the turbulence intensity at the outlet expansion area, however, the calculated results of the *k-ω* SST—RCE model are apparently lower than that of the *k-ω* SST model. That is because the former model takes into account the effect of rotation on the turbulence structure. Under the action of the centrifugal force, the near-wall fluid has to overcome the adverse pressure gradient. But the turbulence intensity becomes weaker and the area grows larger. In particular, the turbulence intensity gradually declines at the outlet.

On the suction surface, the fluid flow is not stable under the rotational effect. The turbulence is more intense at the contact part at the tip of the blade due to the blade structure and the mode of fluid motion. As for the central area, model 2 has lower results than model 1, for the turbulence intensity of model 2 is lower in the central area. In this area, the flu id accelerates towards the surrounding areas. The turbulence formation trend is weak before the fluid reaches the tip of the blade. The trend is also demonstrated in the blade speed nephograms in Figure 12 and Figure 13.

In contrast, in model 1, i.e. the *k-ω* SST model, the turbulence intensity in the expansion area follows the same trend within the blade integrated disk. Besides, model 1 does not consider the effects of rotation and centrifugal force. The above factors contribute to the stronger turbulence intensity and higher calculated results of this model.

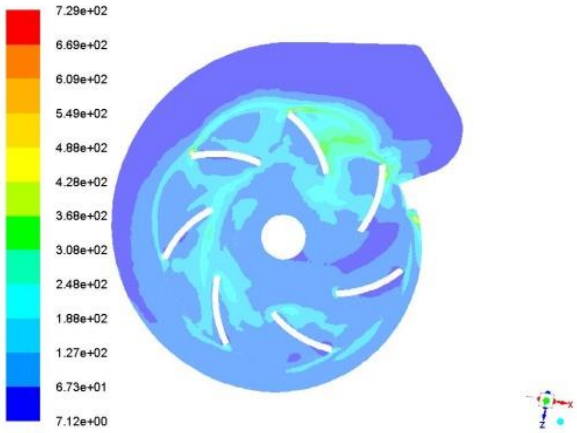

Figure 8. The turbulence intensity of the *k-ω* SST

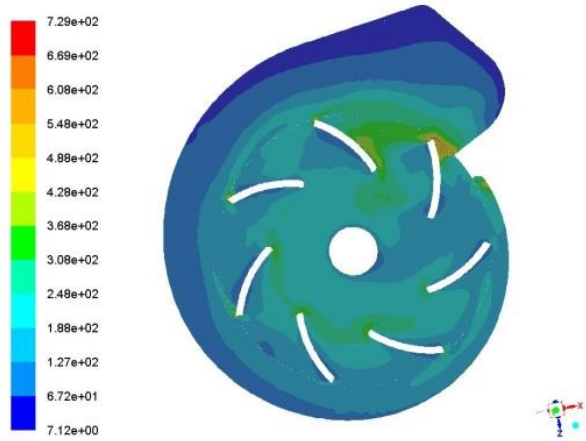

Figure 9. The turbulence intensity of the *k-ω* SST—RCE

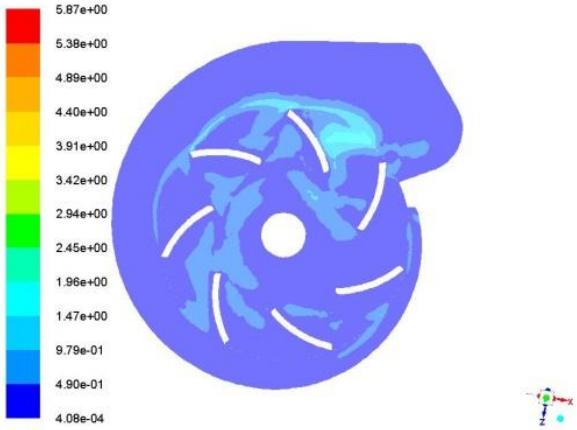

Figure 10. The turbulence viscosity of the *k-ω* SST

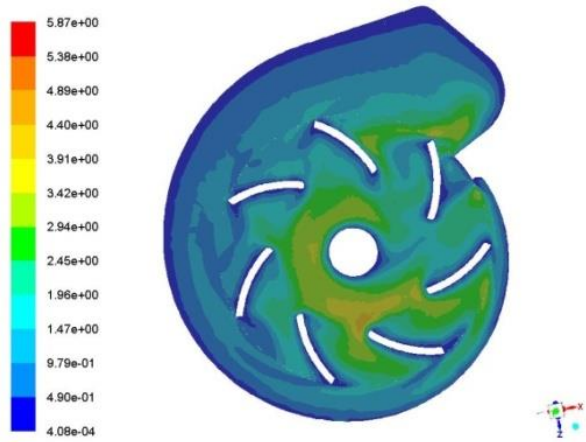

Figure11. The turbulence viscosity of the *k-ω* SST—RCE

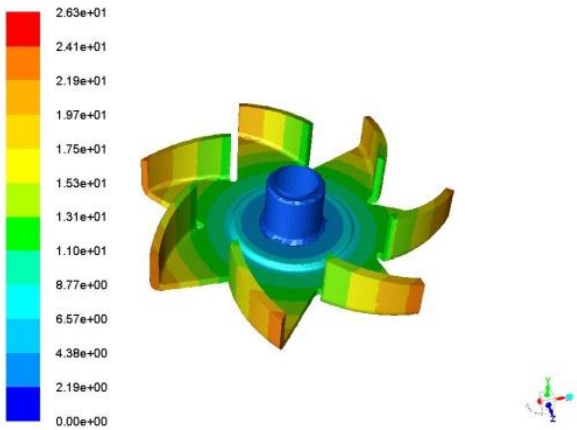

Figure 12. The speed of the blade integrated disk of the *k-ω* SST

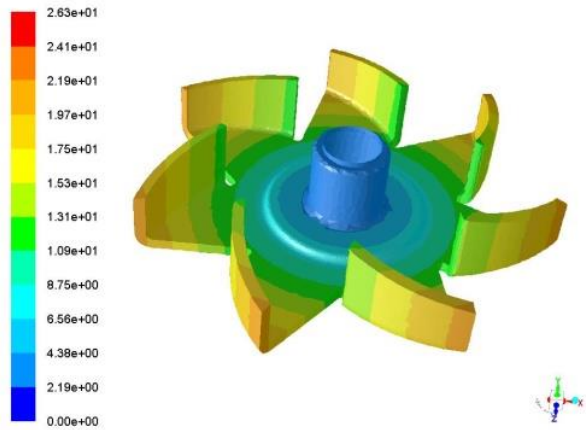

Figure 13. The speed of the blade integrated disk of the *k-ω* SST—RCE

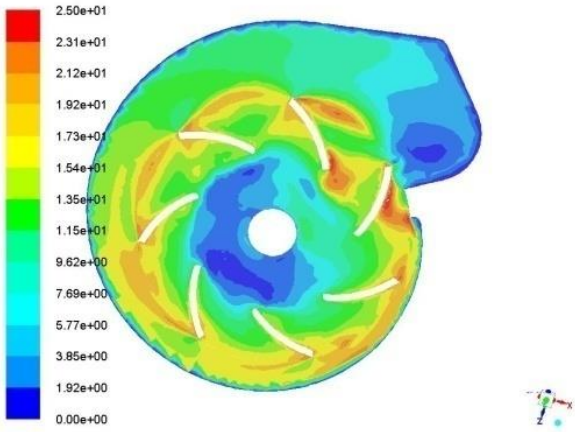

Figure 14. The flow field velocity of the *k-ω* SST

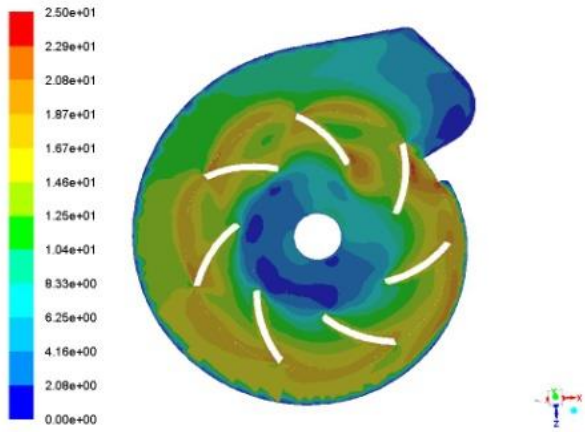

Figure 15. The flow field velocity of the *k-ω* SST—RCE

Flow field velocity analysis.The flow field velocity is shown in Figures 14 and 15. The figures display the cross section at 50% of the blade height in the y-direction of the flow field. The outlet velocity is obviously lower in the nephogram of model 2 than in the nephogram of model 1. The fluid motion is not linear at the outlet. Under the action of rotation and curvature, the normal component of the flow field velocity, coupled with the generation of secondary flow, impedes the mixture of low-velocity fluid and the wake flow and expands the area of low-velocity. The effect persists all the way to the outlet expansion section. In the meantime, the fluid has a tendency to move along the volute wall due to volute curvature and rotation. Considering the impact of the wall, the fluid in model 2 tends less to move forward and is more likely to slow down rapidly. Thus, model 2has a lower outlet velocity, which is consistent with the results of turbulence intensity and viscosity analysis, as well as the calculation results. In the central area, the low-velocity area in model 2 is larger than that in model 1, and the velocity grows significantly after the fluid passes the tip of the blade.

The effect of turbulent kinetic energy.Turbulent kinetic energy is a measure of the development or decline of turbulence. It is ½ of the product of the turbulence velocity fluctuation variance and fluid mass. Figures 16 and 17 are the nephograms of the turbulent kinetic energy calculated by model 1 and model 2. As shown in the figures, model 1 boasts a well-developed turbulence, featuring higher turbulent kinetic energy at the outlet and the central area; model 2, however, has lower turbulent kinetic energy in corresponding areas, a signal of low turbulent velocity. The pattern agrees well with the external characteristic calculation. It also indicates that model 2 is good at capturing turbulence.

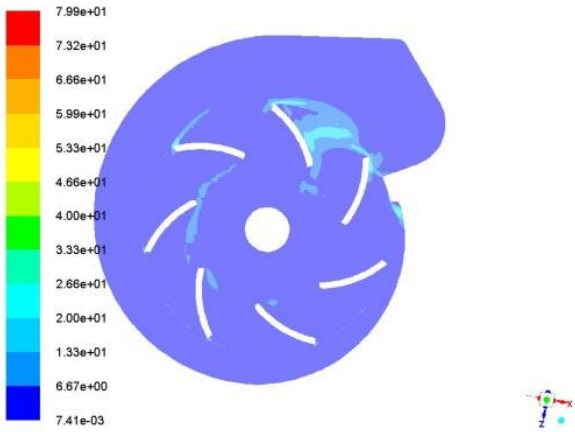

Figure 16. The turbulent kinetic energy of the *k-ω* SST

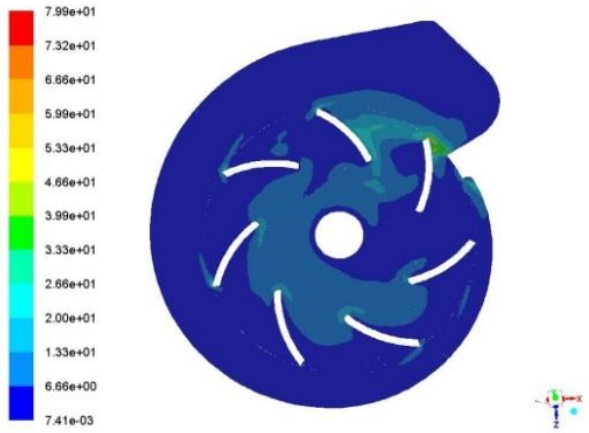

Figure 17. The turbulent kinetic energy of the *k-ω* SST—RCE

5. CONCLUSION

In view of the mode of motion of the flow field in the centrifugal pump, this paper analyzes the advantages and drawbacks of the *k-ω* SST turbulence model when it is adopted for simulation calculation under the working condition of rotational motion and curved walls. On the basis of the model and in the aid of near-wall function, the author corrects the coefficients of the turbulent kinetic energy generation term and dissipation term of the model according to the flow field rotation and curvature effect correction methods proposed by Spalart and Hellsten. The corrected model is applied to the numerical calculation of the centrifugal pump of an automobile motor. In comparison with the original model, the author draws the following conclusions:

1) The calculation results of the external characteristics of a centrifugal pump at a high rotating speed from the improved model are closer to the experimental results. Compared with that of the original model under different flow conditions at a

high rotating speed, the calculation efficiency is improved. In the working condition of a rotating speed of 3,370n/min and a flow of 180L/min, the calculated result of the pump lift is 21.04m, with a calculation error of 0.67%, meaning that the calculation accuracy is improved by 0.3%; the calculated result of efficiency is 26.2%, with a calculation error of 0.76%, meaning that the accuracy is improved by 0.7%.

2) The author compares the calculated results of the two models at 3370n/min and 180L/min, and analyzes the nephograms of the calculation results. In terms of external characteristics, the calculated result of the pump lift in model 2 is smaller than that in model 1, which is closer to the measured value. From the nephograms, it can be seen that the turbulence intensity at the outlet area in model 2 is lower than that in model 1, that the intensity range is greater and that the turbulence intensity at the outlet area lessens along the direction of the fluid motion; in model 2, the speed at the outlet area displayed in the velocity nephogram is also lower than that in model 1. Under the action of rotation and curvature, the normal component of the flow field velocity, coupled with the generation of secondary flow, impedes the mixture of low-velocity fluid and the wake flow and expands the area of low-velocity. The effect persists all the way to the outlet expansion section. The velocity is also gradually decreased along the direction of fluid motion, unlike in model 1, where there is a great velocity gradient. At the same time, the nephograms also show that the fluid at the outlet has a tendency to move along the volute wall, but in model 2, the forward tendency is weak, which is the result of the near-wall treatment of the boundary layer. The turbulence intensity at the outlet is weak, and the flow field velocity is low, so the fluid velocity at the outlet is low, with a low lift. From the above two aspects, it can be seen that the calculated result of pump lift in model 2 is closer to the measured value.

3) When the rotating speed is 2000n/min or lower, the calculated result from the two models are lower than the measured values, and the errors for both pump lift and efficiency are over 3%. In model 1, the maximum error in the calculated result of pump lift is up to 22.36%, thus the result is considered incorrect. The setup of the models under different rotating speeds affects the calculated results. At a low rotating speed, the flow on the interface between the rotating and stationary areas of the pump can no longer be regarded as steady and inhomogeneous, that is, it no longer satisfies the prerequisite for simulation with the MRF (Multiple Reference Frame) model, leading to large errors in the calculated results. As the flow field at a low rotating speed is transient and pulsatile, the calculations regarding the interface should consider the relative sliding of grids and also the interactions between the two areas using a transient calculation method.

REFERENCES

[1] Lang T., Shi W.D., Chen K.Q., et al. (2015). Flow field in forward—extended douboe blades centrifugal pump at different specific speeds, *Transactions of the Chinese Society for Agricultural Machinery*, Vol. 46, No. 12, pp. 89–95.

[2] Rafiee S.E., Sadeghiazad M.M. (2016). Three-dimensional CFD simulation of fluid flow inside a vortex tube on basis of an experimental model- the optimization of vortex chamber radius, *International Journal of Heat and Technology*, Vol. 34, No. 2, pp. 236-244. DOI: 10.18280/ijht.340212

[3] Liu L.L., Sun Z.C., Wan C.L., Wu J.M. (2015). Jet flow field calculation & mechanism analysis on hot-air drying oven based on RNG k-ε model, *International Journal of Heat and Technology*, Vol. 33, No. 1, pp. 77-82. DOI: 10.18280/ijht.330111

[4] Smirnov P.E., Menter F.R. (2009). Sensitization of the SST turbulence model to rotation and curvature by applying the Spalart-Shur correction term, *ASME Journal of Turbomachineru*, Vol. 131, No. 4, pp. 1-8. DOI: 10.1115/1.3070573

[5] Ansys Inc. Ansys CFX-solver theory guide, Canonsburg, 2015.

[6] Johnstion J.P., Halleen R.M., Lezius D.K. (1972). Effects of spanwise rotation on the structure of two-dimensional fully developed turbulent channel flow, *Journal of fluid Mechanics*, Vol. 56, No. 3, pp. 533-557.

[7] Irwin H.P.A.H., Aront S.P. (1975). Prediction of the effect of streamline curvature on turbulence, *Physics of Fluids*, Vol. 18, No. 6, pp. 624-630.

[8] Spalart P.R., Shur M.L. (1997). On the sensitization of turbulence models to rotation and curvature, *Aerospace Science and Technology*, Vol. 1, No. 5, pp. 297-302. DOI: 10.1016/S1270-9638(97)90051-1

[9] Smirnov P.E., Menter F.R. (2009). Sensitization of the SST turbulence model to rotation and curvature by applying the Spalart-Shur correction term, *ASME Journal of Turbomachineru*, Vol. 131, No. 4, pp. 1-8. DOI: 10.1115/1.3070573

[10] Bradshaw P. (1969). The analogy between streamline curvature and buoyancy in turbulent shear flow, *Journal of Fluid Mechanics*, Vol. 36, No. 1, pp. 177-191.

[11] Ansys Inc. Theory Reference. AnsysInc, 2012.

[12] Launder B.E., Priddin C.H., Sharma B. (1977). The calculation of turbulent boundary layers on spinning and curved surfaces, *Journal of Fluids Engineering*, Vol. 99, No. 3, pp. 231-239.

[13] Shur M.L., Strelets M.K., Travin A.K., el al. (2000). Turbulence modeling in rotating and curved channels: assessing the Spalart-Shur correction, *AIAA Journal*, Vol. 38, No. 5, pp. 784-792.

[14] Khodak A., Hirsch C. (1996). Second order non-linear *k-ε* models with explicit effect of curvature and rotation, in *Proc. ECCOMAS-CFD*, New York, USA: Wiley, pp. 690-696.

[15] Hellsten A. (1998). Some improvements in Menter's k-ω SST turbulence model, in Proc AIAA- FDC, Reston, VA, USA, AIAA, pp. 1-11.

NOMENCLATURE

$CD_{k\omega}$	positive portion of the cross-diffusion in ω- transport equation
f_{r1}	rotation/curvature correction function of the SARC model
$r^*, \tilde{r}$	nondimensional criteria of rotation/curvature effects defined in Sec.
S_{ij}	components of the mean strain tensor
ω_{ij}	components of the vorticity tensor
ω_m	components of the system rotation rate vector

ε_{mji}	tensor of Levi–Civita
c_{r1}, c_{r2}, c_{r3}	additional empirical constants of the SA rotation and/or streamline curvature (SARC) model
Ri	Richardson number
C_{rc}	constant coefficient in the rotation and curvature sensitization
R_e	Reynolds number
u_τ	friction velocity
y^+	nondimensional distance from the surface
β^*, γ, β	turbulence-model coefficients
υ	dynamic viscosity
υ_t	turbulent viscosity
k	kinetic energy of turbulence
σ_K, σ_ω	turbulence-model coefficients